Influence of the Different Nanostructures of Acrylonitrile Butadiene Styrene/Multi-Walled Carbon Nanotubes on the Resultant Chemical, Physical and Electrical Properties Following Laser Cutting

Ayub Karimzad Ghavidel[1]*, Jonathan Lawrence[2], Mahmoud Moradi[3]*

[1]Department of Mechanical Engineering, Technical and Vocational University (TVU), Tehran, Iran, a-karimzad@tvu.ac.ir

[2]School of Computing, Engineering & Physical Sciences, University of the West of Scotland (UWS), High Street, Paisley, PA1 2BE, UK

[3]Faculty of Arts, Science and Technology, University of Northampton, Northampton, NN1 5PH, UK mahmoud.moradi@northampton.ac.uk

Abstract

Reported on in depth for the first time herein is the influence of the diverse nanostructures of acrylonitrile butadiene styrene (ABS)/multi-walled carbon nanotubes (MWCNTs) on its chemical, physical and electrical properties after laser cutting. Injection moulding was used to fabricate the nanocomposite samples in various structures with a thickness of 3 mm by adjusting temperature and pressure. The samples' nanostructures were evaluated prior to cutting with a CO_2 laser. Design of experiments (DoE) by a full-factorial method used three levels laser power 45, 55 and 65 W) and the cutting velocity at three levels (4, 8 and 12 mm/s) as independent variables. The findings from this work are significant and support new theories. It was revealed different surface damage modes such as shrink holes, cracks, decomposed smithereens and sink marks. These were affected by the linear energy density criterion which means that the ratio of power to cutting velocity was the governing factor, whilst the effect of primary nanostructures was negligible. Unlike surface damage, the width of heat affected zone (HAZ) was found to depend on the thermal conductivity, which directly relates to the samples' nanostructure. Minimum HAZ was obtained at 0.45 mm for the sample with maximum thermal conductivity equal to 0.23 W/mK. Analysis of the post-laser cut surface and HAZ indicated that the MWCNTs were well dispersed with higher orientation and degrees of distribution. This, naturally, allows the inference that application of low laser energy density accounted for and governed oxidation of these regions. The results show that the nanotexture of the post-laser

cut surface is completely changed in comparison with the as-moulded surface, leading to the lowest reduction in surface electrical resistivity to 3.2 kΩ for the sample produced at a temperature of 220°C and a holding pressure of 70 bar.

1. Introduction

Even though laser cutting is one of the most prevalent non-traditional machining methods in the manufacturing industry [1, 2], the photo-thermal nature of this process presents challenges to the quality of produced parts from two perspectives. The first lies in the dimensions of the kerf created by the laser beam during cutting, which is closely related to the characteristics of workpiece material and process variables such as laser power, cutting velocity, focal distance and assist gas pressure [3-6]. These dependencies lead to the size of produced parts being sensitive to both the material and the adjustable input factors of the process [7, 8]. The second is the thermal performance of laser cutting causes the structure of the cut surface and its vicinity to differ from the base material (BM) [9, 10]. If these undesirable influences are high then the in-service performance of the produced part may be compromised and/or its mechanical durability may be reduced [11-13].

In recent times the drive to produce parts from advanced materials such as polymer-based composites and nanocomposites has increased for many reasons [14]. Composites filled with carbon fibres and carbon nanotubes (CNTs) are of interest because of their unique properties [15-17] which has led to their wide commercial availability in sheet form [18]. Laser cutting of these sheets presents as the ideal manufacturing process due to its speed, non-contact nature and relatively low running cost and, subsequently, many researchers have studied its implementation and methods for control [4, 18, 19].

Of particular note, Ghavidel *et al.* [4] evaluated the laser cutting properties of poly methyl methacrylate (PMMA)/CNTs nanocomposites, finding that kerf width and the straightness of cut edge were strongly influenced by the CNTs concentration, laser power and cutting velocity. In a further study, Ghavidel *et al.* [20] proved a correlation between the surface roughness of the PMMA/CNTs nanocomposite and the CNTs concentration, laser power and cutting velocity. The results of other investigations have shown that higher CNTs concentration

improves the thermal properties of the polymer matrix and influences the laser cut surface texture, producing more precise parts [21, 22].

The literature indicates that the alignment of microfibres or nanofibers in these composites plays a key role in laser cutting outcomes [22-25]. In the laser cutting of CNTs-based nanocomposites the major portion of the generated temperature is transferred along the CNTs axis because the longitudinal thermal conductivity therein is very much more than in the transverse direction [4, 12], leading to consistent asymmetric damage such that the characteristics of laser cutting these materials are heterogeneous [19]. Additionally, the complicated thermal behaviour of carbon fibre-reinforced polymers (CFRPs) and CNTs-based nanocomposites is another factor that effects changes to the morphological and chemical properties after laser cutting operations [26-30]. This manifests as cracks in the heat affected zone (HAZ) and other defects such as striations, delamination, decomposition and sink marks, all of which threaten the mechanical durability of the parts after loading [7, 10, 31]. Tensile strength reduction after laser cutting has also been reported in the literature, stating that this mechanical shortcoming can be attributed to the above-mentioned defects [32-34].

Many researchers utilized laser treatment techniques to create an electrically conductive layer on the surface of CNTs-based nanocomposites, where the incident of different laser sources on the surface of CNTs-based nanocomposites directly terminates a portion of the matrix polymer, leading to the concentration of CNTs increasing up to the percolation threshold of this layer [12, 35-37]. The CNT-CNT contact and forming of a conductive network have been determined to be a mechanism of electron transfer in this layer [23, 38]. It has been stated that the interaction of the laser beam with the surface of the sample makes a viscous film and the impact of the blown assist gas agitates the arrangement of CNTs and forms this network [20, 23].

Despite the potential for and benefits of using laser cutting on the CFRP acrylonitrile butadiene styrene (ABS)/multi-walled carbon nanotubes (MWCNTs) and its ensuing multipurpose applications such as the production of piezo resistors, some of the more important aspects of the underpinning science of this process have not yet been investigated. One such example is since the properties of the nanocomposites are directly influenced by their primary nanostructures, it is expected that the after effects of the laser cutting of these materials in terms of morphology, chemistry and electrical resistivity will be strongly correlated to this, yet this has not been studied. This work addresses this omission by studying the influence of the different nanostructures of ABS/MWCNTs nanocomposite on its chemical, physical and electrical properties after laser cutting for the first time.

3

2. Experimental details

2.1. Materials

Commercially available MWCNTs (Nanostructured and Amorphous Materials Inc.). grown by chemical vapor deposition (CVD). were used in this work and were characterized by an outside diameter (OD) of 30 to 50 nm, an inside diameter (ID) of 5 to 15 nm, a length of 20 μm, purity >95%, a density of 2.1g/cm^3, an aspect ratio of 200/666 and surface area of 90 to 120 m^2/g. The powder ABS graft phase with butadiene SAN was used as a polymer matrix (SV0157-Tabriz Petrochemical Company). The average size of ABS graft and SAN are 100 and 200μm, respectively. Some important mechanical and physical properties of this polymer are tabulated in Table. 1.

Table 1. The properties of polymer matrix.

Property	Unit	Test Conditions	Standard	Typical Value
Melt Flow Index (MFI)	g/10min	200ºC/5Kg	ASTM D-1238	0.5
Izod impact strength	KJ/m^2	---	ASTM D-256	31
Vicut softening point	ºC	50N load	ASTM D-1525	101
Bulk density	g/cm^3	---	---	0.6
Yield point	GPa	---	ASTM D-638	430
Hardness	HRR	@ 23ºC	ASTM D-785	104

2.2. Fabrication of the varied nanostructured nanocomposites

First, the CNTs and polymer matrix were dried at 85ºC for 2 hours in an oven. Next, they were mixed with a co-rotating twin-screw extrusion (ZSK-25; Werner & Pfleiderer GmbH) at the CNTs concentration of 0.8 wt.%. The screw speed of the extruder was set at 150 rpm and the temperatures of the barrel zones were 180, 190, 200 and 215ºC. After extruding and before the injection moulding process, the pellets were dried in an oven at 80ºC for 24 hours. Injection moulding was then carried out (Imen; Paya Machine Sazeh). To create the desired differences in nanostructures, injection temperature (in two levels of 210 and 220ºC) and holding pressure (in three levels of 50, 60, and 70 bar) were considered as variable factors and the other parameters were set according to Table. 2. The dimensions of the samples were 120 × 20 × 3 mm^3 and the injection direction was along the 120 mm side. Table. 3 summarizes the injection moulding conditions for each of the samples.

Table 2. The constant parameters of the injection moulding process.

Parameter	Unit	Amount
Loading pressure	bar	90
Cooling time	s	15
Injection time	s	8
Injection pressure	bar	40
Holding pressure speed	mm/s	8
Injection speed	mm/s	54.3
Mould temperature	ºC	70

Laser cutting was performed using a custom-made laser cutting system (Sahand Laser Company) equipped with a high quality CO_2 laser source (λ=10.6 µm, M^2>1.2 and a Gaussian profile beam)- with a maximum safe power of 120 W and working dimensions of 1200 × 1000 mm^2. The nozzle diameter, focal length, and stand-off distance were 2, 127 and 1.5 mm, respectively. The reason for CO_2 laser selection is the high absorption of the CO_2 wavelength with both the matrix and the fibres [39]. Compressed air with a pressure of 0.28 MPa was used as the assist gas. The focal point of the beam was considered constant in the middle of the sample thickness [4, 40]. The laser beam spot diameter at the focusing point was approximately 180 µm (measured by the supplier). Power in three levels of 50, 65, and 80 W, also cutting velocity in three levels of 4, 8, and 12 mm/s were considered as variables. Preliminary experiments showed that the selected levels lead to complete beam penetration through the whole thickness of the sample, cutting the sample thoroughly. The design of experiments (DOE) was done by the full factorial method and each run of experiments was replicated five times and the average value of results is reported as the final output. The details of the designed experiments and the results are tabulated in Table. 4.

Table 3. The variables parameters of the injection moulding process.

Sample	Process Conditions	
	Injection temperature, T (°C)	Injection pressure, P (bar)
#A	210	50
#B	220	50
#C	210	60
#D	220	60

	#E	210	70
	#F	220	70

Table 4. Experimental layout and obtained results.

No.	Input Parameters				Output Results		
	Category	Laser power (W)	Cutting velocity (mm/s)	Laser Energy Density (W.s/mm)	HAZ (mm)	Kerf width (mm)	Surface electrical resistivity (kΩ)
1	#A	45	4	11.25	0.93	0.81	6.5
2	#A	45	8	5.625	0.82	0.55	7
3	#A	45	12	3.75	0.8	0.48	6.4
4	#A	55	4	13.75	1.1	0.82	6.2
5	#A	55	8	6.875	0.93	0.59	6.8
6	#A	55	12	4.583	0.88	0.49	7.1
7	#A	65	4	16.25	1.25	0.83	6.7
8	#A	65	8	8.125	1	0.69	7.2
9	#A	65	12	5.416	0.93	0.51	7.6
10	#B	45	4	11.25	0.98	0.76	6.3
11	#B	45	8	5.625	0.73	0.63	6.8
12	#B	45	12	3.75	0.71	0.56	7.1
13	#B	55	4	13.75	0.99	0.9	5.9
14	#B	55	8	6.875	0.84	0.68	6.4
15	#B	55	12	4.583	0.8	0.54	6.8
16	#B	65	4	16.25	1.02	0.98	6.3
17	#B	65	8	8.125	0.78	0.68	6.9
18	#B	65	12	5.416	0.75	0.48	7.1
19	#C	45	4	11.25	0.91	0.62	6.4
20	#C	45	8	5.625	0.8	0.53	6.8
21	#C	45	12	3.75	0.68	0.42	7.2
22	#C	55	4	13.75	0.98	0.78	6.1
23	#C	55	8	6.875	0.88	0.59	6.6
24	#C	55	12	4.583	0.7	0.53	7

25	#C	65	4	16.25	1.1	0.82	6.4
26	#C	65	8	8.125	1	0.68	7
27	#C	65	12	5.416	0.76	0.43	7.4
28	#D	45	4	11.25	0.81	0.55	5.3
29	#D	45	8	5.625	0.68	0.37	5.6
30	#D	45	12	3.75	0.57	0.32	6.2
31	#D	55	4	13.75	0.84	0.6	4.9
32	#D	55	8	6.875	0.69	0.41	5.3
33	#D	55	12	4.583	0.56	0.36	6
34	#D	65	4	16.25	0.91	0.62	5.1
35	#D	65	8	8.125	0.81	0.46	5.2
36	#D	65	12	5.416	0.78	0.4	6.1
37	#E	45	4	11.25	0.88	0.7	5.8
38	#E	45	8	5.625	0.81	0.625	6.2
39	#E	45	12	3.75	0.64	0.51	6.4
40	#E	55	4	13.75	0.98	0.81	6.1
41	#E	55	8	6.875	0.85	0.69	6
42	#E	55	12	4.583	0.68	0.54	6.3
43	#E	65	4	16.25	1	0.84	6.2
44	#E	65	8	8.125	0.9	0.72	6.3
45	#E	65	12	5.416	0.8	0.56	6.6
46	#F	45	4	11.25	0.65	0.47	4.2
47	#F	45	8	5.625	0.5	0.36	4.4
48	#F	45	12	3.75	0.45	0.2	5.1
49	#F	55	4	13.75	0.69	0.58	4
50	#F	55	8	6.875	0.52	0.41	3.2
51	#F	55	12	4.583	0.48	0.23	4.6
52	#F	65	4	16.25	0.71	0.62	4.1
53	#F	65	8	8.125	0.58	0.45	3.9
54	#F	65	12	5.416	0.52	0.27	4.2

2.3. Characterization methods

The microscopic and chemical structure of the samples before and after laser cutting were investigated by a field-emission scanning electron microscope (FE-SEM) fitted with a energy-dispersive X-ray spectroscope (EDS) (MIR3; TESCAN). To determine the effect of the injection moulding process on the morphology of each prepared sample they were firstly fractured after storing within a liquid N_2 bath, then the apparent cross-section of the sample (which is perpendicular to injection flow) was investigated by the FE-SEM. The chemical characteristics of the post-laser cut surfaces (the surfaces which were in contact with the laser beam) were determined by EDS using the mapping mode on the area with the dimensions of 250×250 μm^2. The nanotexture of these surfaces was also examined using the FE-SEM micrographs at different points.

The chemical alterations in HAZ were evaluated by EDX line analysis on 10 points of a line perpendicular to the cutting edge with a length of 1 mm, in such a way that it includes at least 2 and 8 points of the base nanocomposite and HAZ, respectively. The width of the HAZ was also measured at least in 20 points along the cut edge using an optical microscope (BX61; Olympus Ltd.) at a magnification of 200× and the average of these values was reported as HAZ width.

A similar approach was followed to measure the kerf width at the laser beam entrance and the exit, and the average of these two dimensions was considered to be the kerf width. After measuring the width of the kerf the samples were cut along the kerf to get accessibility to the laser cut surfaces. Then two sites were Au coated by sputtering on the surfaces with the dimensions of 1×3 mm^2, in accordance with the previous work of Ghavidel *et al.* [41].

A multi-meter equipped with a four-pin probe (3458A; Agilent Inc.) was used to measure the electrical resistivity of post-laser cut surfaces by connecting the probes on the Au coated sites. The thermal conductivity measurement of the as-moulded samples was conducted as described by Mohammadi *et al.* [42].

3. Results and discussion

3.1. Microscopic structure and characteristics of the as-moulded nanocomposites

Fig. 1 shows FE-SEM micrographs from the cross-section of the fabricated samples by injection moulding. According to the microscopic investigations, increasing the injection temperature from 210 to 220ºC decreases the size and numbers of CNTs agglomerates [43, 44], because the matrix polymer becomes more viscous, resulting in more energy transmits to

agglomerates [44, 45], and enhancing dispersion and distribution degree [46, 47]. Moreover, higher injection pressure has the same influence on the dispersion condition. More FE-SEM micrographs can be seen in the Supplementary Information, **Fig. S1**.
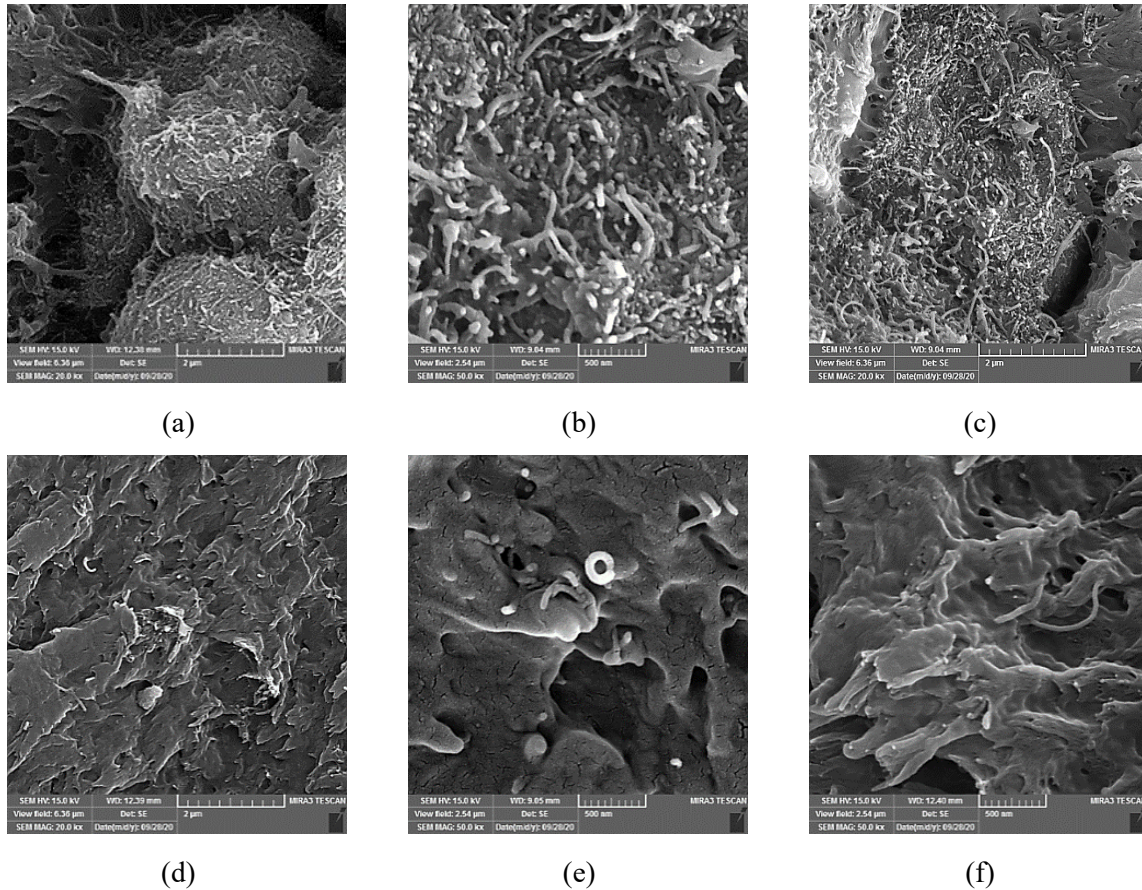

Fig. 1. Nanostructure of prepared samples (FE-SEM images) by different injection molding temperature and pressure: (a) #A, (b) #B, (c) #C, (d) #D, (e) #E and (f) #F.

According to the obtained nanostructure after the molding operation, it seems that the specimens prepared at the temperature of 220 °C will have better thermal conductivity [48, 49]. To objectively realize this hypothesis, the thermal conductivity of the samples was measured in the perpendicular direction to the injection flow at a constant temperature of 80 °C, as described in reference [42] and the results are shown in Fig. 2. As can be seen in this figure, the thermal conductivity for the samples fabricated at the temperature of 220 °C is much higher than the samples moulded at the temperature of 210 °C (especially for the holding pressure of 70 bar). Improving the dispersion of CNTs confirmed by FE-SEM micrographs (Fig. 1) is the main reason for this finding. Trifle increase in thermal conductivity is observed by higher injection pressure in Fig. 2. Regarding the improvement

of the CNTs alignment along the injection flow, this finding can be justified, which has already been discussed in references [50, 51]. Analysis of variance (ANOVA) for the result of thermal conductivity can be seen in the Supplementary Information, Table. S1. Regards to the p-value statistics obtained lower than 0.05, from a statistical point of view both factors of injection temperature and holding pressure are effective on thermal conductivity by the level confidence of 90%.
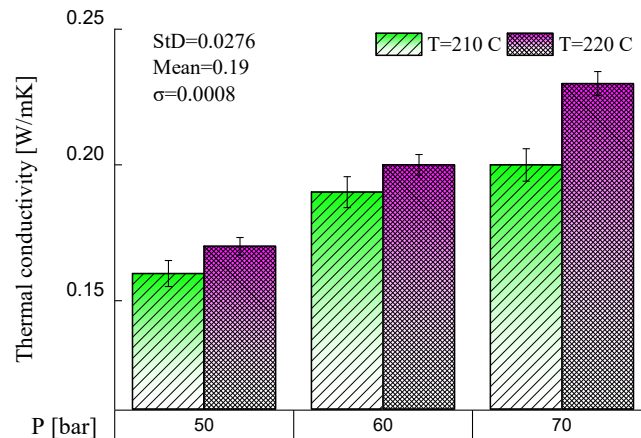
Fig. 2. The effect of different nanostructures created by injection moulding conditions on the thermal conductivity of samples.

3.2. Microscopic structure of the post-processed surfaces of the nanocomposites

The morphology of some surfaces (FE-SEM images) after laser cutting is depicted in Fig. 3. As this surface is in contact with a laser beam and first melted and then re-solidified, thermodynamic phenomena is happened in this layer, affecting its final texture. Fig. 3(a-d) is related to sample-#A which has been cut with the power of 45 W and a cutting velocity of 12 mm/s. As is obvious, only some holes have been created on the surface of sample-#A, appearing due to the transition of the surface layer from viscous phase to viscoelastic state [7, 10]; moreover, nanocomposite agglomerates with a high concentration of CNTs are observed that the base polymer has been destroyed by increasing the temperature and these agglomerates have been reproduced by solidification of the viscous layer. Part of the decomposed polymer in the cut path covered the outer surface of these agglomerates and the nanotubes were trapped inside them. Fig. 3(e-h) portrays the cut surface of sample-#A with a power of 65 W and a cutting velocity of 4 mm/s. In this case, too, only some holes can be seen on the surface, whose dimensions are larger compared to Fig. 3(a-d). Regarding the agglomerates, increasing the power and reducing the cutting velocity led to their smaller size. FE-SEM images of the cut

surface of sample-#F with the power of 45 W and cutting velocity of 12 mm/s are shown in Fig. 3(i-l). As can be seen in this regard, post-processed defects such as shrink holes are very less, and the distribution of agglomerates is better than in the two earlier discussed samples. To discuss this issue, it is necessary to define an index called the linear energy density (laser energy density), which is equal to the power of the laser beam to the cutting velocity (laser energy density=P/V) [52-54]. The increase in this ratio indicates the intensification of the transmitted energy rate to the material undercutting. According to the microscopic finding, it seems that at a constant laser energy density, higher thermal conductivity leads to rapid transfer of heat from the cut vicinity, forming a surface with fewer defects [7, 10]. Of course, this interpretation is preliminary and it is necessary to discuss other microscopic findings. Fig. 3(m-p) illustrates the surface of sample-#F, after cutting with the power of 65 W and a cutting velocity of 4 mm/s. The existence of micron-scale cracks and holes and very large agglomerates with a narrow size distribution are the most important points to be mentioned about this category. Based on the definition of laser energy density factor, a general summary of microscopic studies of cut surfaces can be presented: for a low laser energy density (such as a power of 45 W and cutting velocity of 12 mm/s), increasing the sample's thermal conductivity caused by its microscopic nanostructure results better conditions and surface texture, but for a high laser energy density (such as a power of 65 W and cutting velocity of 4 mm/s) the thermal conductivity did not play a role and a lot of damage occurs on the surfaces after laser cutting. In general, it can be concluded that the influence of laser energy density on the microscopic structure of surfaces is more than on the samples' nanostructure.

(a): #A, P=45 W, V= 12 mm/s (b): #A, P=45 W, V= 12 mm/s (c): #A, P=45 W, V= 12 mm/s (d): #A, P=45 W, V= 12 mm/s

(e): #A, P=65 W, V=4 mm/s

(f): #A, P=65 W, V=4 mm/s

(g): #A, P=65 W, V=4 mm/s

(h): #A, P=65 W, V=4 mm/s

(i): #F, P=45 W, V= 12 mm/s

(j): #F, P=45 W, V= 12 mm/s

(k): #F, P=45 W, V= 12 mm/s

(l): #F, P=45 W, V= 12 mm/s

(m): #F, P=65 W, V=4 mm/s

(n): #F, P=65 W, V=4 mm/s

(o): #F, P=65 W, V=4 mm/s

(p): #F, P=65 W, V=4 mm/s
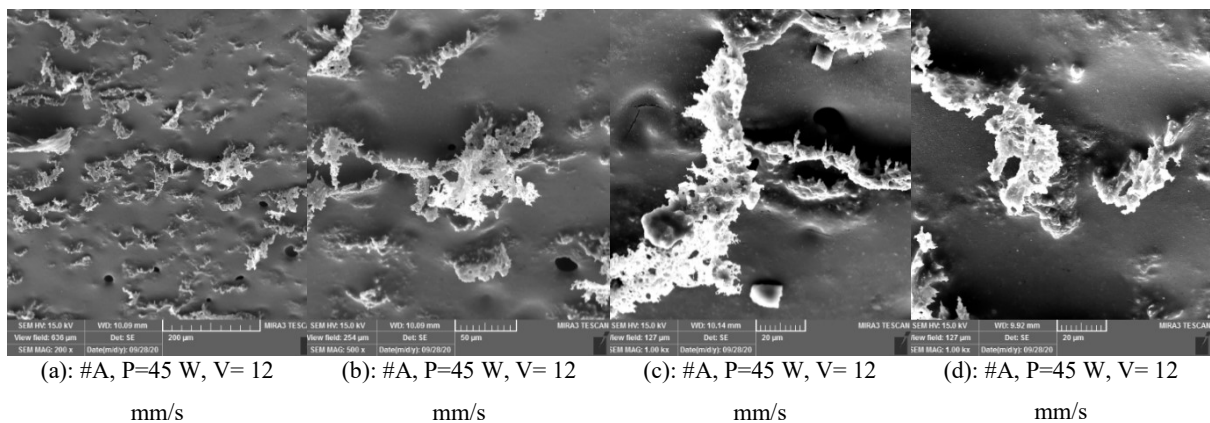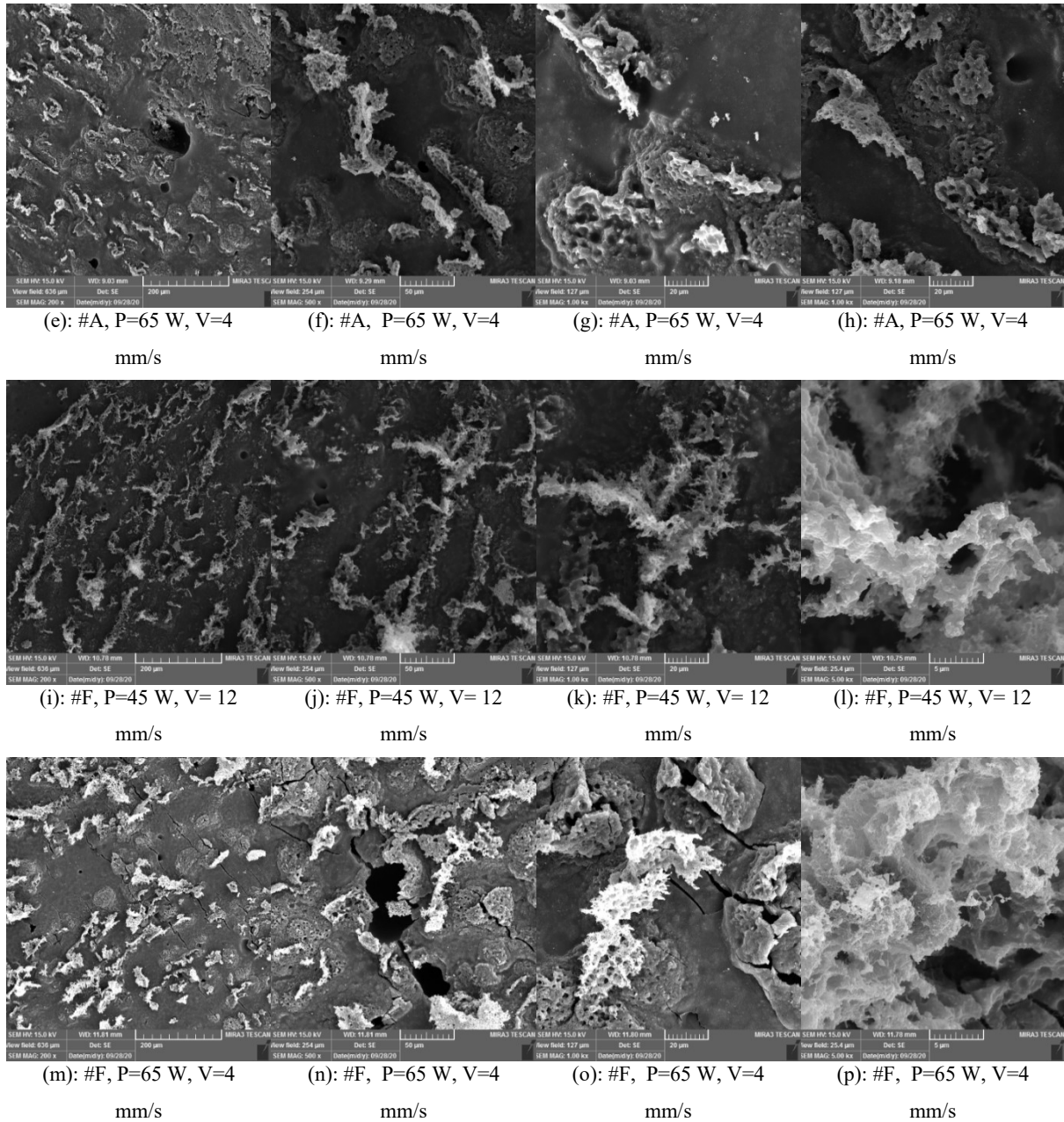
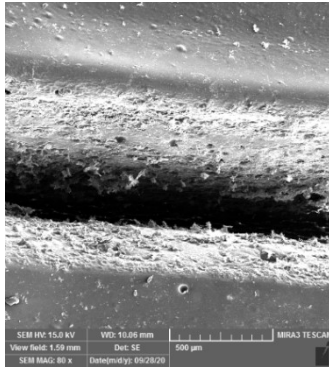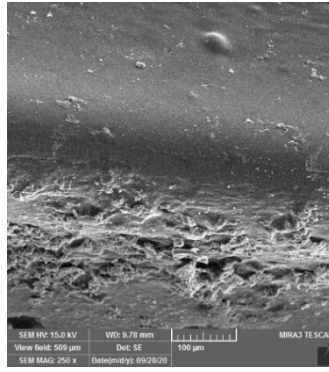Fig. 3. The effect of laser cutting variables and microscopic structure of samples on the texture of the surface. Each image's primary structure and cutting conditions are written below them.

3.3. Microscopic and chemical analysis of the heat affected zone

The HAZ is the area of nanocomposite that has not been thermally degraded during laser cutting and has only experienced some alternation in chemical and physical properties as a result of being exposed to relatively high temperatures [4, 7]. The HAZ is located between the cut edge and the unaffected base nanocomposite, distinguished by different colours under the optical or SEM microscopic [4]. Fig. 4 shows several FE-SEM images of HAZ for different samples. Fig. 4(a-c) corresponds to sample-#A, which was cut with a power of 45 W and a

velocity of 12 mm/s (laser energy density= 3.75). In Fig. 4(a) and (b) the overflow of viscous material in the form of burr can be seen around the cutting edge. Fig. 4(c) also proves the existence of a micro-crack in the HAZ. Fig. 4 (d-f) is also related to sample-#A, which was produced at the power and cutting velocity of 65 W and 4 mm/s (laser energy density= 16.25), respectively. In these figures, there are deep sink marks around the edges in addition to the cracks and forming a significant burr, showing that laser energy density intensification led to more damage in the HAZ. Similar results were obtained in the microscopic investigation of other samples-#A, fabricated by different laser cutting variables. It seems that for samples with the same structure and thermal conductivity, an increase in laser energy density rises damages in HAZ [1, 54, 55]. Fig. 4(g-i) indicates FE-SEM micrographs for sample-#F, cut with the power and cutting velocities of 45 and 12 (laser energy density= 3.75), respectively. According to these micrographs, there are only shallow sink marks around the edge, and cracks can not be seen in the HAZ. FE-SEM micrographs for sample-#F, cut with the power and cutting velocity of 65 and 4 (laser energy density= 16.25), respectively are presented in Fig. 4(j-l). Long-length microcracks and medium-depth sink marks are in the HAZ, but their numbers are very low compared to earlier samples. These observations confirm that a higher thermal conductivity in contrast to the reference [12] and in agreement with the reference results [4] not only reduces the defects in the HAZ but also prevents the expansion of this region by eliminating the thermal focus. If the generated heat during laser cutting is not transmitted quickly away from the cut edges, the temperature has risen sharply and the conditions for phase-transition in this area and the production of secondary damages are prepared. As a general conclusion from the microscopic studies, it can be summarized that the structure and morphology of the cut surfaces are strongly dependent on laser energy density, while the defects and the development of HAZ were influenced by the thermal conductivity of the sample, and the role of laser energy density on it is weak [4, 10].
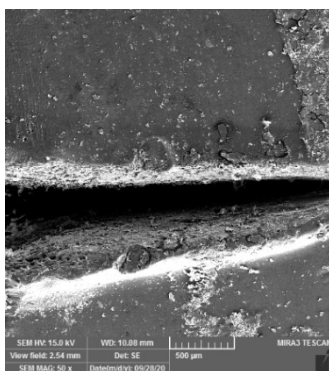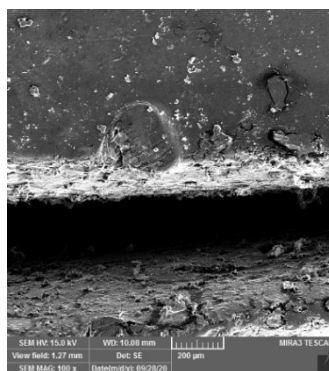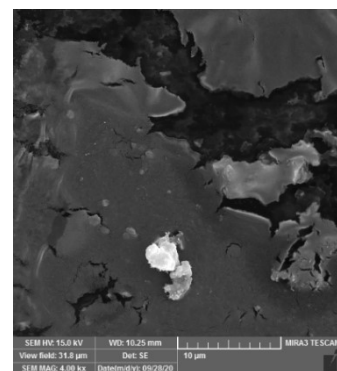
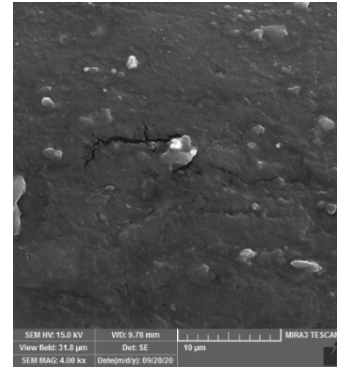(a): #A, P=45 W, V= 12 mm/s   (b): #A, P=45 W, V= 12 mm/s   (c): #A, P=45 W, V= 12 mm/s
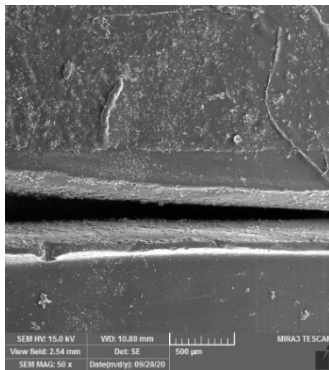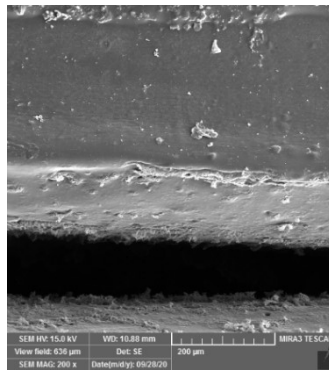
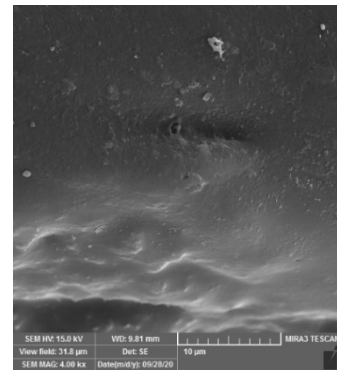(d): #A, P=65 W, V= 4 mm/s   (e): #A, P=65 W, V= 4 mm/s   (f): #A, P=65 W, V= 4 mm/s
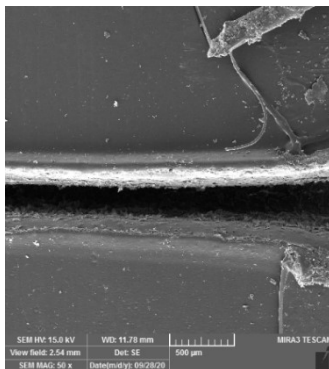
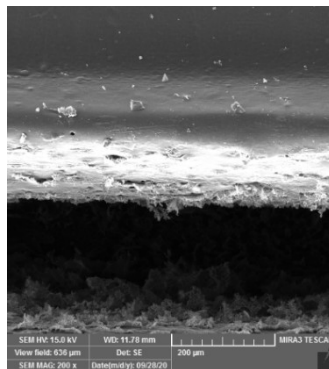(g): #F, P=45 W, V= 12 mm/s   (h): #F, P=45 W, V= 12 mm/s   (i): #F, P=45 W, V= 12 mm/s
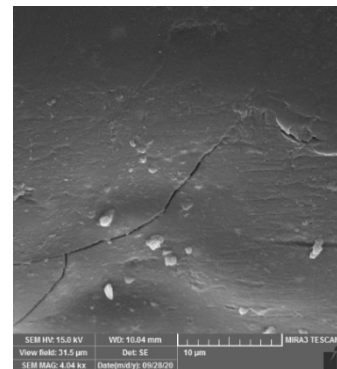
(j): #F, P=65 W, V= 4 mm/s   (k): #F, P=65 W, V= 4 mm/s   (l): #F, P=65 W, V= 4 mm/s

Fig. 4. The morphology and microscopic structure of HAZ. Each image's primary structure and cutting conditions are written below them.

Fig. 5 shows the effect of laser cutting variables and the primary nanostructure of samples on the width of HAZ. As is evident, for structures prepared by injection pressure of 50 bar, an increase in cutting velocity limits the expansion of HAZ, regardless of the injection temperature. Higher beam motion velocity decreases laser energy density, causing low thermal energy to transmit, consequently, HAZ width is reduced [1]. The power has the same effect as the velocity for both samples injected at 210 and 220 °C temperatures, which increasing laser energy density by power leads to broad HAZ [1, 4]. The width of HAZ for sample-#B is smaller

than sample-#A, confirming an improvement in dispersion and alignment of CNTs through higher injection temperature has a significant influence on the thermal conductivity of specimens and the developing HAZ along the injection flow [56-58]. The formation or size decrease of CNT agglomerates has a close relationship with the injection moulding temperature. In the past years, it has been proven that by increasing the injection temperature, the size of agglomerates is reduced to a great extent and leads to the improvement of the thermal conductivity of nanocomposites [44, 45, 47, 59, 60], reflected in the results of measuring the thermal conductivity (see Fig. 2). More CNTs separation from agglomerates and dispersion in matrix augments thermal conductivity (see Fig. 2), transmitting the generated heat quickly and hindering HAZ enlargement.

Fig. 5(b) and (c) depict the results of HAZ for the samples prepared by the injection pressure of 60 and 70 bar, respectively. Here, the effect of cutting velocity and power is exactly the same as the samples-#A and #B that were explained. The noteworthy point is the decreasing trend of HAZ with increasing pressure and injection temperature, verifying rising the thermal conductivity along the injection due to more orientation of CNTs, a major part of the produced heat is transferred in this direction and the broadening of the HAZ is prevented. Higher injection pressure in addition to more dispersion, aligns the CNTs along the injection flow, creating anisotropic thermal properties in such a way that higher conductivity is obtained in the direction of injection, where orientation occurs [12, 49, 61]. Therefore, quick heat transmitting in a parallel direction of kerf growth reduces the required thermal focus to form a wide HAZ [4, 22]. ANOVA results for the HAZ width were tabulated in the Supplementary Information, Table. S2. According to this table, all of the input factors including laser power, cutting velocity, and the primary nanostructure of the nanocomposites are effective on the width of HAZ. The interaction of the samples' nanostructure with the parameters of laser cutting is meaningful, but the interaction between power and cutting velocity is trivial.
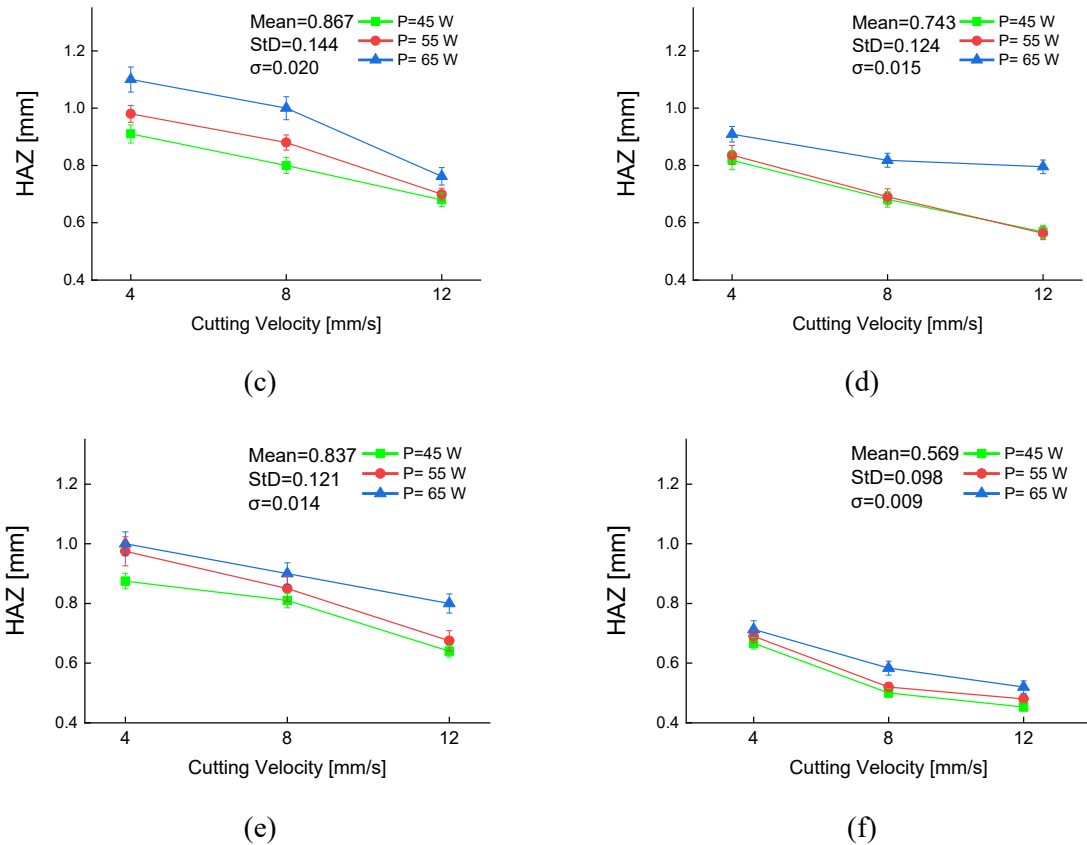

(a)   (b)
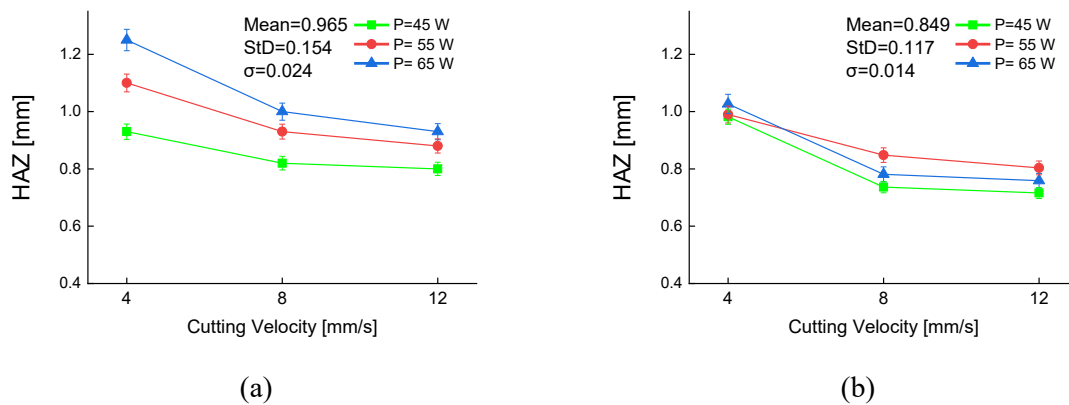
Fig. 5. The effect of laser cutting variables on HAZ width for the samples with different microscopic structures: (a) #A, (b) #B, (c) #C, (d) #D, (e) #E and (f) #F.

3.3. Chemical analysis of intact and post-laser cut surfaces

EDX analysis results for intact and post–laser cut surfaces of samples-#A and #B were tabulated in Table 1. Herein, three elements of carbon, oxygen, and silicon were detected. Of course, the presence of hydrogen is certain, but due to its small atomic number, EDX is not able to detect it. Therefore, here reported values are relative and valid only to compare the current research samples. ABS polymer chains and CNTs contain carbon but the source of silicon may be pollution during the compounding or injection molding process. Oxygen may be coming from the metal oxide impurity of CNTs [62, 63]. Any change in O and C amount can be examined from two perspectives [64]: I) The oxidation of the carbon of the polymer chains or the free carbons around the nanotubes. II) Destruction of a part of polymer on the surface layer and concentrating the CNTs proportion. It can be observed that all samples have experienced a significant reduction in the carbon percentage of the surface layer, even though the concentration of CNTs has been increased after the laser beam incident, confirmed by FE-SEM micrographs. The thermal stability of carbon nanotubes is very higher than that of the polymeric matrix (ABS). The applied linear energy is not enough to decompose the CNTs, so
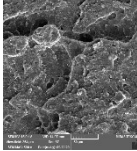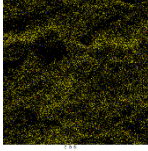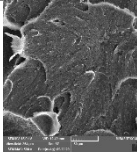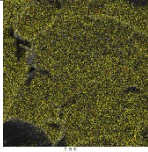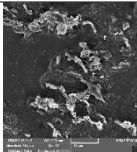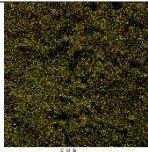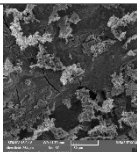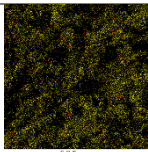
the part of the matrix directly evaporates, resulting increase in the population of CNTs on the cut surface or increasing the CNTs concentration [65]. This point expresses that the oxidation role is more highlighted than concentrating. The results clarify the surface of sample-#F was oxidated less due to its large thermal conductivity. However, the oxidation was intensified by growing laser energy density in these categories. It can be summarized that the production of nanostructure with higher injection temperature and pressure and reducing laser energy density are accounted as the influential parameters to govern the oxidation of the post-processed surface.

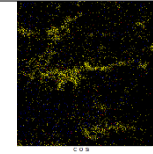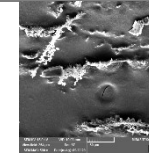## 3.4. Multi-point chemical results of the heat affected zone

The results of EDX analysis of HAZ for four samples with FE-SEM images were tabulated in Table 3. The oxygen percentage is the maximum at the cutting edge and gradually decreases by moving away from it, indicating carbon oxidation is high at the edge due to the intensity of temperature and has decreased by moving away from the edge towards the BM. In the case of sample-#A, conducted by the power of 65 W and cutting velocity of 4 mm/s, the oxygen is 4.4% in the base structure, increasing along HAZ toward the edge and reaching exactly 15.18% on the edge. This trend implies significant oxidation at this level of energy (laser energy density=16.25) where the phase transition has occurred certainly.

For the same cutting conditions, by changing the nanostructure from #A to #F, the oxygen element changes from 11.47% (base-nanocomposite) to 12.56% (cutting edge). Indeed, the oxidation in this category is the same as the sample-#A, but its intensity is much lower. It seems that the higher thermal conductivity of sample-#F compared to #A causes the heat to transmit rapidly, subsequently less oxidation. Similar changes have occurred at a power of 45 W and a cutting velocity of 12 mm/s (laser energy density=3.75) for #A and #F, with the difference that the oxidation is relatively lower at this level of laser energy density. As a brief overview of this discussion, to control HAZ oxidation, #F microscopic structure is recommended with the simultaneous use of low laser energy density.

Table. 1. EDX analysis results for intact structures and post-processed surfaces

Materials		Injection parameters		Laser cutting parameters			EDX results						Surface texture	Elements distribution
							Element wt.%			Elements A%				
Symbols		Temperature	pressure	Power [W]	Cutting Velocity [mm/s]	laser energy density	C	O	Si	C	O	Si	SEM micrograph	Map Image
Raw samples	#A	210	50	---	---	---	93.17	5.83	1	95.1	4.46	0.44		
	#F	220	70	---	---	---	94.61	5.17	0.22	95.97	3.94	0.1		
Processed samples	#A	210	50	65	4	16.25	86.04	12.94	1.77	88.36	9.98	1.66		
	#F	220	70	65	4	16.25	87.01	12.02	0.97	90.03	9.04	0.93		

#A	210	50	45	12	3.75	86.64	12.63	0.73	88.23	10.3	1.47		
#F	220	70	45	12	3.75	87.29	11.07	1.64	89.1	10.02	0.88		
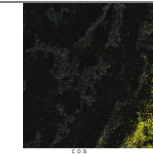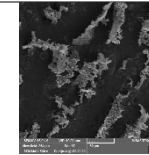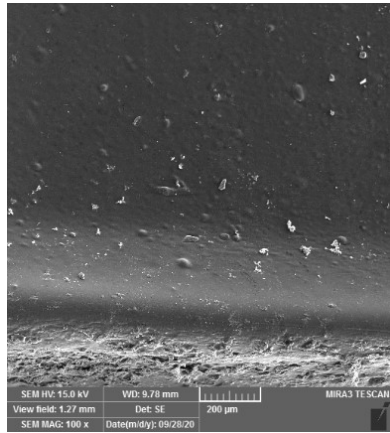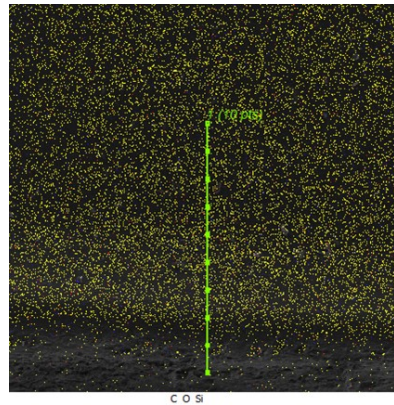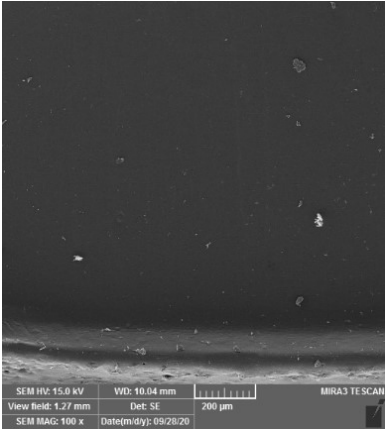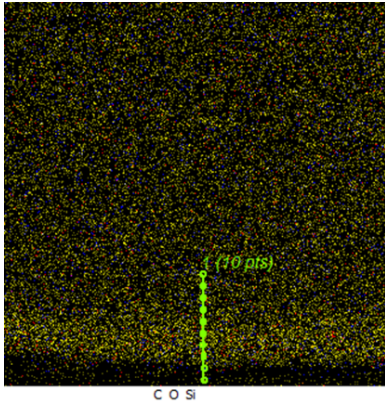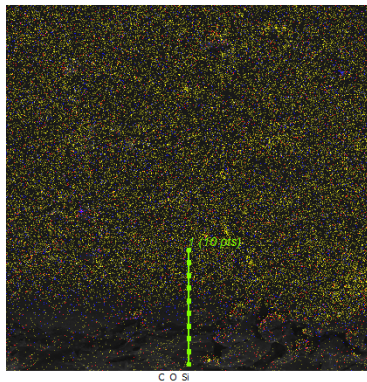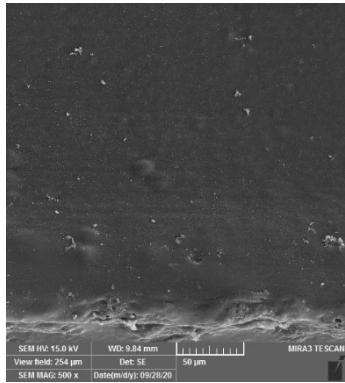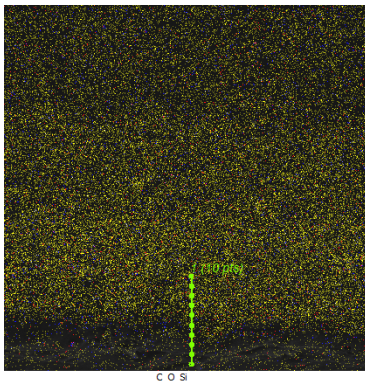
Table. 2. Multi-point EDX results of HAZ

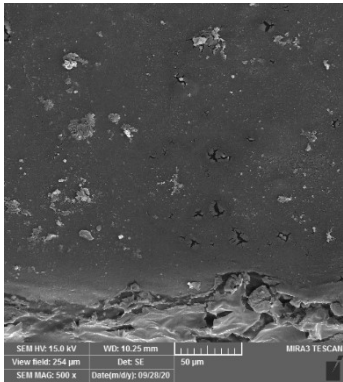| Symbole	Laser cutting parameters		Point	EDX results						SEM image	Map analysis image
	Power [W]	Cutting Velocity [mm/s]		Element wt.%			Element A%				
				C	O	Si	C	O	Si		
#A	65	4	1	95.12	4.4	0.48	96.44	3.35	0.21		
			2	93.28	5.96	0.76	95.07	4.46	0.47		
			3	93.01	6.34	0.65	94.84	5.01	0.15		
			4	92.8	6.68	0.52	94.56	5.24	0.2		
			5	92.4	7.33	0.27	94.27	5.61	0.12		
			6	91.1	8.39	0.51	92.71	7.2	0.09		
			7	89.03	10.42	0.55	92.8	7.15	0.15		
			8	86.7	12.61	0.69	90.46	9.42	0.12		
			9	86.15	13.07	0.78	90.12	9.1	0.78		

			10	84.31	15.18	0.51	88.39	10.48	1.13		
#F	65	4	1	87.89	11.47	0.64	90.97	8.75	0.28		
			2	87.82	11.62	0.56	90.69	8.82	0.49		
			3	87.8	11.68	0.42	90.65	8.93	0.42		
			4	87.79	11.71	0.5	90.48	8.74	0.78		
			5	87.75	11.78	0.47	90.47	9.05	0.48		
			6	87.92	11.73	0.35	90.84	9.01	0.15		
			7	87.67	12.01	0.32	91.08	8.41	0.51		
			8	87.02	12.32	0.66	91.96	7.16	0.88		
			9	87.16	12.47	0.37	92.03	7.6	0.37		
			10	87.1	12.56	0.34	92.15	6.18	1.67		
#A	45	12	1	93.1	5.61	1.29	95.43	3.12	1.45		
			2	92.81	5.63	1.56	95.35	3.18	1.47		
			3	92.1	5.6	2.3	95.31	3.26	1.43		
			4	92.34	5.73	1.93	95.28	3.28	1.44		
			5	91.88	5.81	2.31	95.2	3.41	1.39		
			6	91.76	5.76	2.48	95.31	3.52	1.17		
			7	91.94	5.92	2.14	95.02	3.68	1.3		
			8	91.12	5.88	3	94.82	3.91	1.27		
			9	91.02	5.94	3.04	94.63	4.17	1.2		

|			10	90.92	6.01	3.07	94.18	4.43	1.39		
#F	45	12	1	95.43	3.6	0.97	0.6	7.06	92.34		
			2	95.4	3.54	1.06	0.72	6.92	92.36		
			3	95.34	3.57	1.09	0.68	6.22	92.1		
			4	95.3	3.53	1.17	0.91	7.06	92.03		
			5	95.42	3.62	0.96	0.84	7.21	91.95		
			6	95.46	3.81	0.73	0.76	7.26	91.98		
			7	95.31	3.76	0.93	0.83	7.31	91.86		
			8	95.01	3.91	1.08	0.87	7.4	91.73		
			9	94.94	4.01	1.05	0.73	7.62	91.65		
			10	94.91	4	1.09	0.81	7.68	91.51		

3.5. Kerf width analysis

The incident of the laser beam with the sample removes away a portion of material when it cuts through, known as the kerf, which its width depends on the material type and other in-process factors [4, 7, 19]. Fig. 6 presents the effect of laser cutting variables and different samples' nanostructure on the kerf width. As can be seen in Fig. 6(a) which corresponds to sample-#A, the kerf becomes more narrow by increasing the cutting velocity for an injection temperature of 210°C. This finding is in agreement with other researchers' results [4, 19]. Accelerating the beam movement or lower laser power reduces the laser energy density and input heat to the sample [1]. Thus, the width of the melted or destroyed area is significantly limited. On the other hand, for sample-#B (see Fig. 6(b)) this trend was repeated exactly, but the kerf width was significantly decreased. As discussed in the case of HAZ, higher injection temperature miniatures the agglomerates of CNTs and finally improves the thermal conductivity of samples. In this situation, the generated heat by the beam incident is transmitted quickly and limited the development of the kerf [4, 22].

Fig. 6(c) shows the results of kerf measurement for sample-#C. In these figures, the graphs follow the same trend of sample-#A (see Fig. 6(a)) and sample-#B (see Fig. 6(b)), but the kerf width is meaningfully decreased compared to #A and #B. It is probably due to the change in the cutting mechanisms from molten to destructive, as explained in reference [7]. There are two validated mechanisms in laser cutting of polymer-base materials: (i) The beam melts a whole portion of the cutting path and the blowing of assist gas empties the molten material, called the molten mechanism. (ii) the heat on the cutting path goes as high as the material is directly destroyed without melting, entitled the destructive mechanism. The comparison between the average results for injection pressure of 50 and 60 bar shows that the kerf width is smaller for the prepared sample by 60 bar, approving that an improvement in CNTs alignment along the injection flow (in-line with kerf expansion) helps manipulate the width of the kerf [19].

Fig. 6(e) and Fig. 6(f) is related to the samples produced at the injection pressure of 70 bar. Forming and development of kerf dimension at this level of pressure are directly dependent on injection temperature. For sample-#E the values of kerf width are as close as to others, but for sample-#F a drastic decrease in kerf size is observed. The reason for this phenomenon in addition to the anisotropic change in thermal conductivity is rooted in the rheological alterations of the nanocomposite [66-68]. The aforementioned injection conditions are responsible for the greatest effect in reducing the CNTs' agglomerates, increasing the number of individual CNTs, and significantly improving alignment [44, 45, 47]. These alterations

decrease the melt flow index (MFI) of nanocomposites which is one of the important rheological properties, making it difficult to evacuate the molten material from the cutting path, leading to kerf width reduction. However, these alterations can be attributed to changes in the nanocomposite cutting mechanism from molten to destructive, as mentioned earlier [7]. Table. S2 in the Supplementary Information is related to the ANOVA results of kerf width. The obtained statistics of p-values in this table indicate that only the interaction of the samples' nanostructure with the laser power is ineffective on the kerf width.
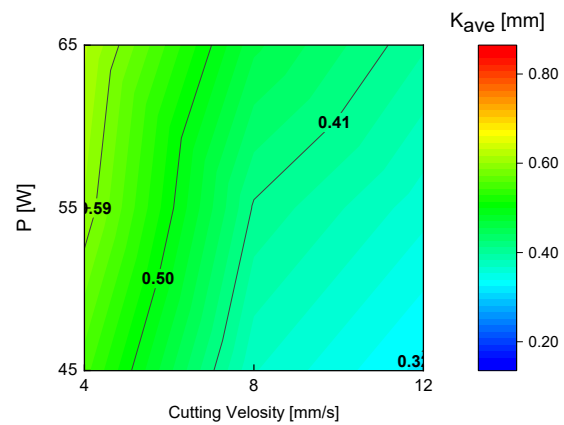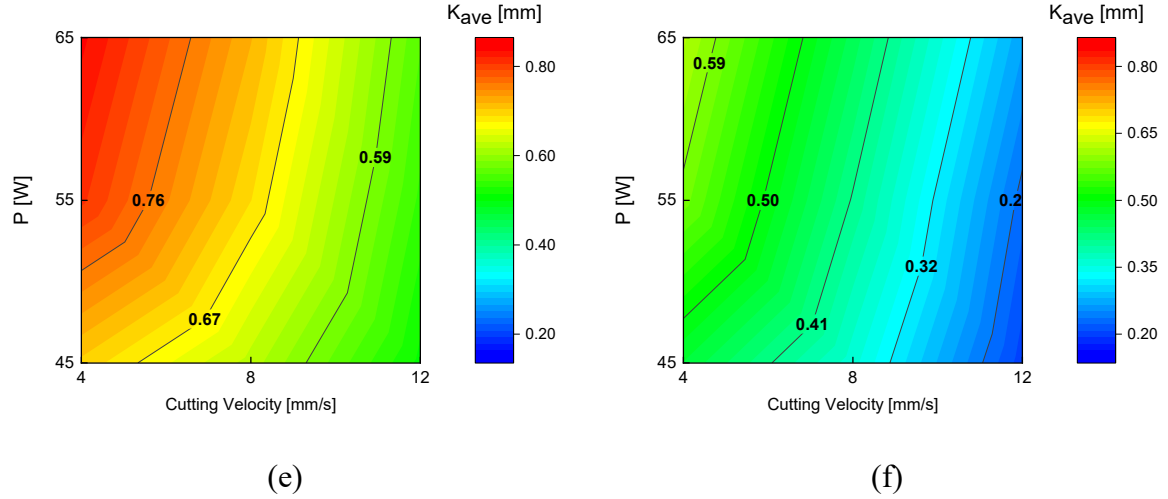

(a)

(b)

(c)

(d)

(e)   (f)
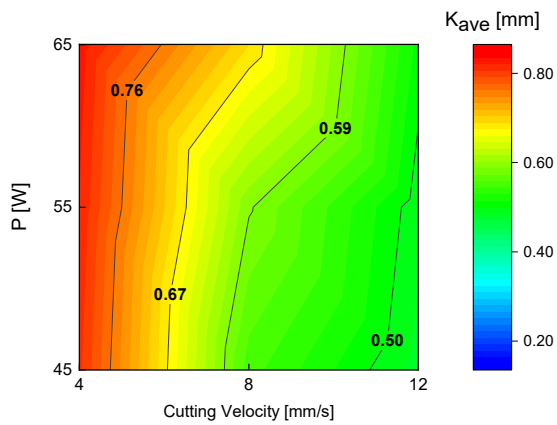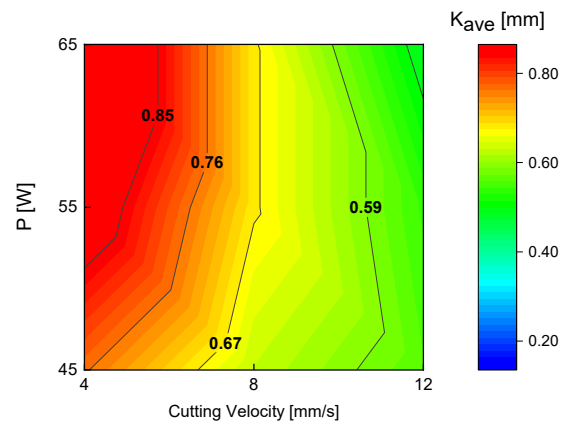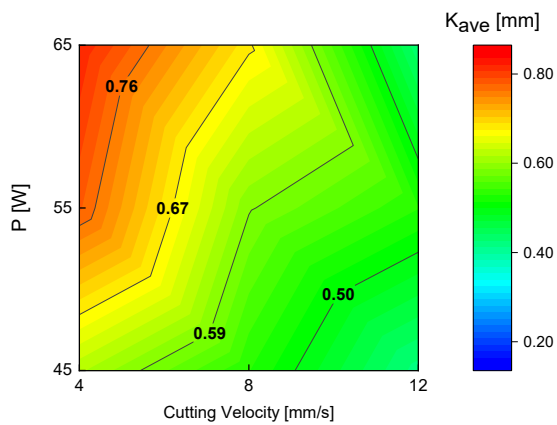
Fig. 6. The effect of laser cutting variables on kerf width for the samples with different microscopic structures: (a) #A, (b) #B, (c) #C, (d) #D, (e) #E and (f) #F.

3.6. Electrical resistivity post-laser cutting

There are valid references, which report a notable decrease in the electrical resistivity of the surface of the CNT-based nanocomposites after laser cutting, which was used to produce the piezoresistors [35, 38, 69]. This change is restricted to the surface layer in which blowing of the assist gas in the viscous state increases the CNT-CNT contact and their entanglement [20, 38], forming a conductive network to carry electrons [70]. But recent studies account for three reasons for this event [65]: (i) generation of a new layer and a CNTs network on the surface; (ii) Increasing the CNTs Concentration up to the percolation threshold; and (iii) Chemical reaction in the surface structures. Microscopic studies by this research show that high CNTs concentration is mainly responsible to create the conductivity among the mentioned hypothesis. In this way, most of the polymer is destroyed by the incident of the laser beam, but the CNTs are not damaged because of their high thermal stability [7, 69, 71-73]. As such, destroying the polymer chains enriches the layer from CNTs concentration, and conductivity comes into existence.
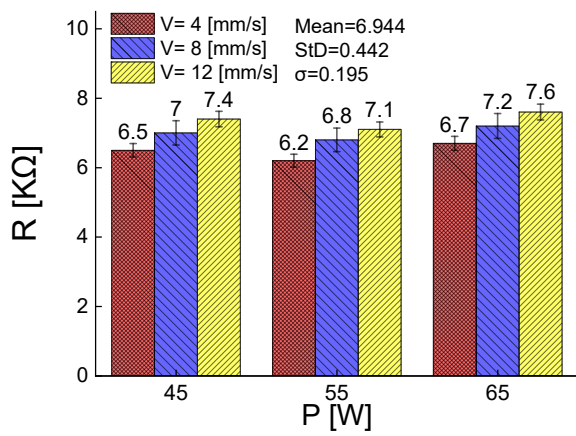
Fig. 7 shows the electrical resistivity of different samples. As is clear, the resistivity is diminished by high cutting velocity for all studied structures, which is in agreement with the results of other research [23, 37]. Increasing the cutting velocity reduces laser energy density and the conditions for the complete destruction of the polymer chains and the increase of the nanocomposite concentration on the surface are not provided. Meanwhile, the polymer chains wrap more around the CNTs, weakening the effective CNT-CNT contact and electron transfer phenomena [65, 70].

The results of resistivity measurements for sample-#A presented in Fig. 7(a). As can be seen in this figure, the prepared sample at the temperature of 210ºC has a higher resistivity. This is due to the more miniaturizing of the agglomerates at higher injection temperatures [44, 47]. In this category, first, the resistivity is reduced by increasing the power from 45 to 55 W because of more polymer destruction. According to the microscopic investigations, higher power makes thinner the wrapped surrounding polymer chains CNTs which act as an insulator around a conductive wire, do not allow to happen CNT-CNT contact. FE-SEM micrographs (Fig. 3) prove appropriate redistribution of CNTs is another factor to decrease the resistivity significantly. The notable point is the rising resistivity by increasing the power to 65 W contrary to the above-mentioned interpretation. Herein, more oxidation of the surface's elements (according to the EDX analysis), reproduction of secondary agglomerates, and surface damages such as sink marks, cracks, and adverse CNTs distribution are the parameters to enhancing the electrical resistivity, contrary to expectations. For all powers, higher cutting velocity causes to rise in the electrical resistivity due to more covering the CNTs through the polymer chains. The results for sample-#B were reported in Fig. 7(b). The trend changes in this category are like #A, but the amounts of resistivities are lower. High injection temperature has decreased the primary CNT agglomerations and created a better dispersion degree, caused to achieve a higher electrical conductivity.

Fig. 7(c) and (d) are related to the results of the sample-#C and sample-#D categories, respectively. A trifle decrease in electrical resistivity is observed in comparison with #A and #B categories, which probably happened due to the improvement in CNTs dispersion and separation, however, the influence of in-process variables is the same.

Fig. 7(e) and (f) show the electrical resistivity of the post-processed surface of the sample-#E and sample-#F categories, respectively. The effect of laser cutting inputs is similar to the previous nanocomposites, but there is a significant reduction in resistivity of the sample-#F. As discussed earlier, the nanostructure of sample-#F was allocated the first rank from the point of view of the dispersion and distribution degree because the molding at the highest temperature and pressure, led to the lowest electrical conductivity; hence, in addition to the effective in-process parameters, the intact samples' nanostructure is very determinative. Low surface damages, enhancement in the rearrangement of CNTs, decrease in oxidation, and low CNTs covering with the decomposed polymer are accounted as such factors, providing a situation to reach the lowest electrical resistivity equal to 3.2 kΩ for sample-#F (laser power of 55 W and cutting velocity of 8 mm/s). ANOVA results for the electrical resistivity of post-processed surfaces were reported in Table. S4 in the Supplementary Information. As is directly
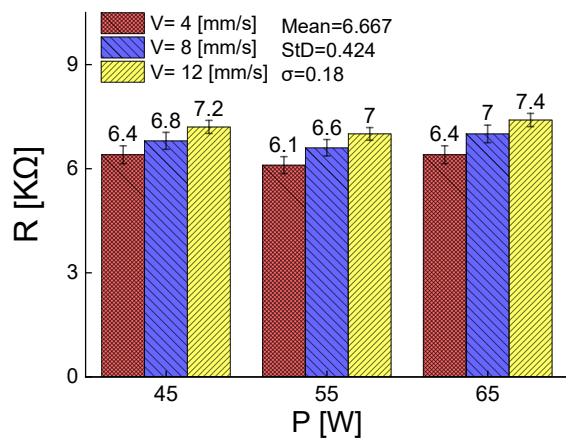
inferred from the p-values, only the interaction effect of the laser power and cutting velocity on the resistivity is improbable.
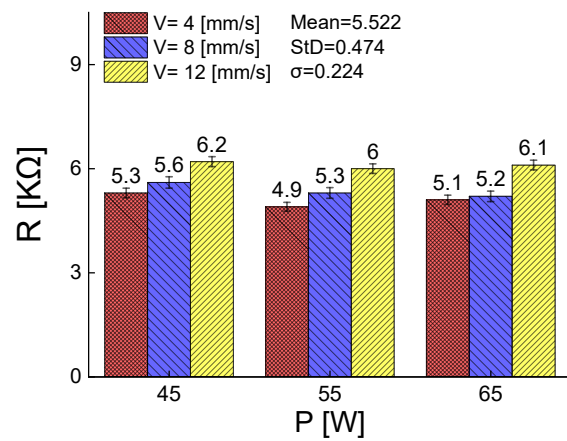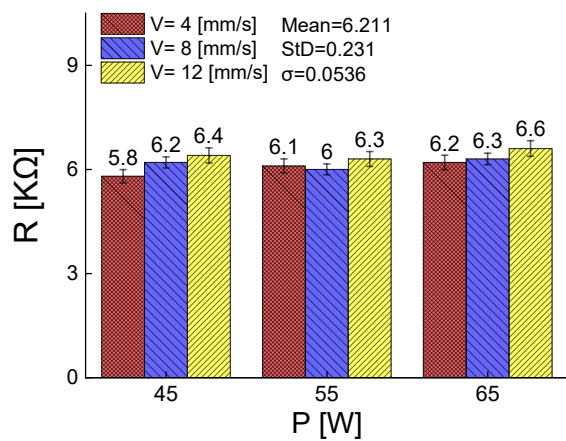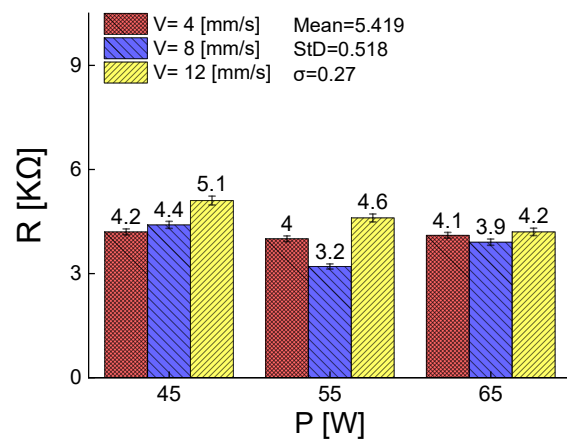

(a)
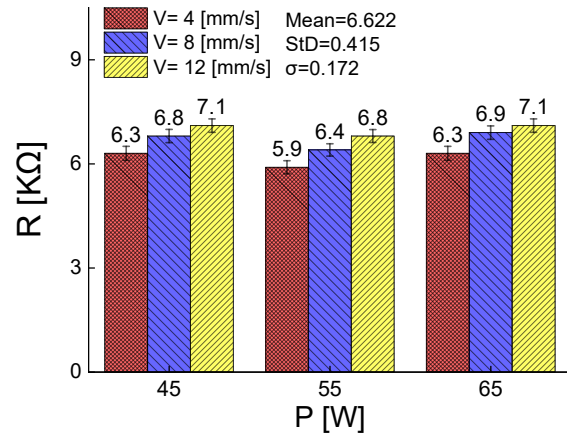
(b)

(c)

(d)

(e)

(f)

Fig. 7. The influence of laser cutting variables and different samples' nanostructure on the electrical resistivity of post-processed surface: (a) #A, (b) #B, (c) #C, (d) #D, (e) #E and (f) #F

4 Conclusions

The effect of the different structures of acrylonitrile butadiene styrene (ABS)/multi-walled carbon nanotubes (MWCNTs) on its chemical, physical and electrical properties after laser cutting was investigated. To fabricate the dissimilar nanostructures an injection moulding process was applied considering the different temperatures and pressures. The prepared samples were cut using the CO_2 laser cutting process at different powers and cutting velocities. The results indicated that the laser cutting outputs of the nanocomposites are intensely overshadowed by their primary nanostructure.

The texture of the post-processed surface is significantly affected by laser energy density, and the influence of primary microscopic structure is negligible. The lowest possible value of laser energy density is recommended to reduce surface damage as such shrink holes, cracks, decomposed pieces, and sink marks.

The width of HAZ and kerf are directly dependent on the thermal conductivity of samples, caused by the microscopic structure. The high dispersion and distribution degree of CNTs and small-size agglomerates leads to an increase in the thermal conductivity of nanocomposite, diminishing the thermal focus, and hindering the development of HAZ and kerf.

According to the EDX analysis results, more separation of the CNTs from the main agglomerates, high dispersion and distribution degree, and decreasing laser energy density are the factors to govern the oxidation of the post-processed surface and HAZ.

The minimum electrical resistivity was obtained at 3.2 kΩ for the samples prepared by injection temperature of 220 ºC and holding pressure of 70 bar. The primary structure of this sample was determined as the reason for this substantial reduction.

As a general conclusion, to attain an ideal condition for cutting, including the lowest HAZ and kerf, the maximum surface electrical conductivity, and limiting the defects of post-processed surface, firstly, the nanostructure of nanocomposite should contain the least agglomerates and the maximum dispersion degree; secondly, the minimum possible linear energy density of in-process should be followed.

References

[1] M. Moradi, O. Mehrabi, T. Azdast, K.Y. Benyounis, Enhancement of low power CO2 laser cutting process for injection molded polycarbonate, Opt. Laser Technol. 96 (2017) 208-218. https://doi.org/10.1016/j.optlastec.2017.05.022.

[2] M. Moradi, E. Golchin, Investigation on the effects of process parameters on laser percussion drilling using finite element methodology; statistical modelling and optimization, Lat. Am. J. Solids Struct. 14 (2017) 464-484. https://dx.doi.org/10.1590/1679-78253247.

[3] E. Haddadi, M. Moradi, A.K. Ghavidel, A.K. Ghavidel, S. Meiabadi, Experimental and parametric evaluation of cut quality characteristics in CO_2 laser cutting of polystyrene, Optik. 184 (2019) 103-114. https://doi.org/10.1016/j.ijleo.2019.03.040.

[4] A.K. Ghavidel, T. Azdast, M.R. Shabgard, A. Navidfar, S.M. Shishavan, Effect of carbon nanotubes on laser cutting of multi-walled carbon nanotubes/poly methyl methacrylate nanocomposites, Opt. Laser Technol. 67 (2015) 119-124. https://doi.org/10.1016/j.optlastec.2014.10.003.

[5] M. Li, S. Li, X. Yang, Y. Zhang, Z. Liang, Effect of lay-up configuration and processing parameters on surface quality during fiber laser cutting of CFRP laminates, J. Adv. Manuf. Technol. 100(1) (2019) 623-635. https://doi.org/10.1007/s00170-018-2728-9.

[6] S. Genna, E. Menna, G. Rubino, V. Tagliaferri, Experimental investigation of industrial laser cutting: the effect of the material selection and the process parameters on the kerf quality, Appl. Sci. 10(14) (2020) 4956. https://doi.org/10.3390/app10144956.

[7] A.K. Ghavidel, M. Zadshakoyan, Comprehensive study of laser cutting effects on the properties of acrylonitrile butadiene styrene, J. Adv. Manuf. Technol. 97(9) (2018) 3637-3653. https://doi.org/10.1007/s00170-018-2166-8.

[8] A. Sharma, V. Yadava, Experimental analysis of Nd-YAG laser cutting of sheet materials–A review, Opt. Laser Technol. 98 (2018) 264-280. https://doi.org/10.1016/j.optlastec.2017.08.002.

[9] G. Casalino, M. Moradi, M.K. Moghadam, A. Khorram, P. Perulli, Experimental and numerical study of AISI 4130 steel surface hardening by pulsed Nd: YAG laser, Mater. 12(19) (2019) 3136. https://doi.org/10.3390/ma12193136.

[10] A. Karimzad Ghavidel, M. Shabgard, H. Biglari, Microscopic and mechanical properties of semi-crystalline and amorphous polymeric parts produced by laser cutting, J. Appl. Polym. Sci. 133(44) (2016). http://dx.doi.org/10.1002/app.44179.

[11] A. Maeda, Y. Jin, T. Kuboki, Light press of sheet metal edge for reducing residual stress generated by laser cutting considering mechanical properties and intensity of residual stress, J. Mater. Process. Technol. 225 (2015) 178-184. https://doi.org/10.1016/j.jmatprotec.2015.05.019.

[12] S. Gbordzoe, S. Yarmolenko, S. Kanakaraj, M.R. Haase, N.T. Alvarez, R. Borgemenke, P.K. Adusei, V. Shanov, Effects of laser cutting on the structural and mechanical properties of carbon

nanotube assemblages, Mater. Sci. Eng. B. 223 (2017) 143-152. https://doi.org/10.1016/j.mseb.2017.06.010.

[13] I.A. Choudhury, S. Shirley, Laser cutting of polymeric materials: An experimental investigation, Opt. Laser Technol. 42(3) (2010) 503-508. https://doi.org/10.1016/j.optlastec.2009.09.006.

[14] S. Veličković, B. Stojanović, L. Ivanović, S. Miladinović, S. Milojević, Application of nanocomposites in the automotive industry, Mobil. Veh. Mech. 45(3) (2019) 51-64. https://doi.org/10.24874/mvm.2019.45.03.05.

[15] T. McNally, P. Pötschke, Polymer-carbon nanotube composites: Preparation, properties and applications, Elsevier, 2011.

[16] M. Harussani, S. Sapuan, G. Nadeem, T. Rafin, W. Kirubaanand, Recent applications of carbon-based composites in defence industry: A review, Def. Technol. (2022). https://doi.org/10.1016/j.dt.2022.03.006.

[17] M. Ates, A.A. Eker, B. Eker, Carbon nanotube-based nanocomposites and their applications, J. Adhes. Sci. Technol. 31(18) (2017) 1977-1997. https://doi.org/10.1080/01694243.2017.1295625.

[18] A.R. Bucossi, J.E. Rossi, B.J. Landi, I. Puchades, Experimental design for CO2 laser cutting of sub-millimeter features in very large-area carbon nanotube sheets, Opt. Laser Technol. 134 (2021) 106591. https://doi.org/10.1016/j.optlastec.2020.106591.

[19] A.K. Ghavidel, M. Shabgard, T. Azdast, Influence of Alignment and Dispersion Pattern of Carbon Nanotubes in the Polycarbonate and Polystyrene Matrixes on Laser Cutting Workability, J. Laser Micro Nanoeng. 11(2) (2016). http://dx.doi.org/10.2961/jlmn.2016.02.0020.

[20] A. K. Ghavidel, A. Navidfar, M. Shabgard, T. Azdast, Role of CO_2 laser cutting conditions on anisotropic properties of nanocomposite contain carbon nanotubes, J. Laser Appl. 28(3) (2016) 032006. http://dx.doi.org/10.2351/1.4947491.

[21] A.K. Ghavidel, M. Zadshakouyan, Dimensional accuracy of CNTs/PMMA parts and holes produced by laser cutting, Int. J. Mech. Eng. 11(10) (2017) 1736-1741. http://scholar.waset.org/1307-6892/10008158.

[22] F. Al-Sulaiman, B. Yilbas, M. Ahsan, CO_2 laser cutting of a carbon/carbon multi-lamelled plain-weave structure, J. Mater. Process. Technol. 173(3) (2006) 345-351. https://doi.org/10.1016/j.jmatprotec.2005.12.004.

[23] A.K. Ghavidel, T. Azdast, M. Shabgard, A. Navidfar, S. Sadighikia, Improving electrical conductivity of poly methyl methacrylate by utilization of carbon nanotube and CO_2 laser, J. Appl. Polym. Sci. 132(42) (2015). http://dx.doi.org/10.1002/app.42671.

[24] P. Mucha, P. Berger, R. Weber, N. Speker, B. Sommer, T. Graf, Calibrated heat flow model for the determination of different heat-affected zones in single-pass laser-cut CFRP using a cw CO_2 laser, Appl. Phys. 118(4) (2015) 1509-1516. https://doi.org/10.1007/s00339-014-8932-z.

[25] M. Li, S. Li, X. Yang, Y. Zhang, Z. Liang, Fiber laser cutting of CFRP laminates with single-and multi-pass strategy: A feasibility study, Opt. Laser Technol. 107 (2018) 443-453. https://doi.org/10.1016/j.optlastec.2018.06.025.

[26] F. Lundström, K. Frogner, M. Andersson, Analysis of the temperature distribution in weave-based CFRP during induction heating using a simplified numerical model with a cross-ply representation, Compos. B. Eng. 223 (2021) 109153. https://doi.org/10.1016/j.compositesb.2021.109153.

[27] F. Lundström, K. Frogner, M. Andersson, Numerical modelling of CFRP induction heating using temperature-dependent material properties, Compos. B. Eng. 220 (2021) 108982. https://doi.org/10.1016/j.compositesb.2021.108982.

[28] A.K. Pathak, H. Garg, M. Singh, T. Yokozeki, S.R. Dhakate, Enhanced interfacial properties of graphene oxide incorporated carbon fiber reinforced epoxy nanocomposite: a systematic thermal properties investigation, J. Polym. Res. 26(2) (2019) 1-13. https://doi.org/10.1007/s10965-018-1668-2.

[29] Y. Zare, K.Y. Rhee, Following the morphological and thermal properties of PLA/PEO blends containing carbon nanotubes (CNTs) during hydrolytic degradation, Compos. B. Eng. 175 (2019) 107132. https://doi.org/10.1016/j.compositesb.2019.107132.

[30] M. Hassanzadeh-Aghdam, R. Ansari, Thermal conductivity of shape memory polymer nanocomposites containing carbon nanotubes: A micromechanical approach, Compos. B. Eng. 162 (2019) 167-177. https://doi.org/10.1016/j.compositesb.2018.11.003.

[31] M. Li, G. Gan, Y. Zhang, X. Yang, Thermal damage of CFRP laminate in fiber laser cutting process and its impact on the mechanical behavior and strain distribution, Arch. Civ. Mech. Eng. 19(4) (2019) 1511-1522. https://doi.org/10.1016/j.acme.2019.08.005.

[32] S. Ullah, X. Li, G. Guo, A.R. Rodríguez, D. Li, J. Du, L. Cui, L. Wei, X. Liu, Influence of the fiber laser cutting parameters on the mechanical properties and cut− edge microfeatures of a AA2B06− T4 aluminum alloy, Opt. Laser Technol. 156 (2022) 108395. https://doi.org/10.1016/j.optlastec.2022.108395.

[33] A.J. Guerra, J. Farjas, J. Ciurana, Fibre laser cutting of polycaprolactone sheet for stents manufacturing: A feasibility study, Opt. Laser Technol. 95 (2017) 113-123. https://doi.org/10.1016/j.optlastec.2017.03.048.

[34] A. Noskov, P. Loskutova, R. Yanbaev, A.K. Gilmutdinov, The mechanical properties of carbon fiber reinforced polymers after laser processing, Laser Phys. 29(9) (2019) 096002. https://doi.org/10.1088/1555-6611/ab344c.

[35] E. Padovano, M. Bonelli, A. Veca, E. De Meo, C. Badini, Effect of long-term mechanical cycling and laser surface treatment on piezoresistive properties of SEBS-CNTs composites, React. Funct. Polym. 152 (2020) 104601. https://doi.org/10.1016/j.reactfunctpolym.2020.104601.

[36] C.J. Long, N.D. Orloff, K.A. Twedt, T. Lam, F. Vargas-Lara, M. Zhao, B. Natarajan, K.C. Scott, E. Marksz, T. Nguyen, Giant surface conductivity enhancement in a carbon nanotube composite by

ultraviolet light exposure, ACS Appl. Mater. Interfaces. 8(35) (2016) 23230-23235. http://dx.doi.org/10.1021/acsami.6b04522.

[37] G. Colucci, C. Beltrame, M. Giorcelli, A. Veca, C. Badini, A novel approach to obtain conductive tracks on PP/MWCNT nanocomposites by laser printing, RSC Adv. 6(34) (2016) 28522-28531. https://doi.org/10.1039/C6RA02726A.

[38] A. Caradonna, C. Badini, E. Padovano, A. Veca, E. De Meo, M. Pietroluongo, Laser treatments for improving electrical conductivity and piezoresistive behavior of polymer–carbon nanofiller composites, Micromachines. 10(1) (2019) 63. https://doi.org/10.3390/mi10010063.

[39] D. Herzog, P. Jaeschke, O. Meier, H. Haferkamp, Investigations on the thermal effect caused by laser cutting with respect to static strength of CFRP, Int. J. Mach. Tools Manuf. 48(12-13) (2008) 1464-1473. https://doi.org/10.1016/j.ijmachtools.2008.04.007.

[40] J.P. Davim, N. Barricas, M. Conceicao, C. Oliveira, Some experimental studies on CO_2 laser cutting quality of polymeric materials, J. Mater. Process. Technol. 198(1-3) (2008) 99-104. https://doi.org/10.1016/j.jmatprotec.2007.06.056.

[41] A.K. Ghavidel, M. Zadshakoyan, M. Arjmand, G. Kiani, A novel electro-mechanical technique for efficient dispersion of carbon nanotubes in liquid media, Int. J. Mech. Sci. 207 (2021) 106633. https://doi.org/10.1016/j.ijmecsci.2021.106633.

[42] A. Mohammadi, A. Shojaei, S.S. Khasraghi, A.K. Ghavidel, Synthesis of high-reinforcing-silica@ nanodiamond nanohybrids as efficient particles for enhancement of mechanical, thermal, and rolling resistance of styrene-butadiene rubber, Polymer. 255 (2022) 125122. https://doi.org/10.1016/j.polymer.2022.125122.

[43] A. Navidfar, T. Azdast, A. Karimzad Ghavidel, Influence of processing condition and carbon nanotube on mechanical properties of injection molded multi-walled carbon nanotube/poly (methyl methacrylate) nanocomposites, J. Appl. Polym. Sci. 133(31) (2016). http://dx.doi.org/10.1002/app.43738.

[44] G.R. Kasaliwal, S. Pegel, A. Göldel, P. Pötschke, G. Heinrich, Analysis of agglomerate dispersion mechanisms of multiwalled carbon nanotubes during melt mixing in polycarbonate, Polymer. 51(12) (2010) 2708-2720. https://doi.org/10.1016/j.polymer.2010.02.048.

[45] I. Alig, P. Pötschke, D. Lellinger, T. Skipa, S. Pegel, G.R. Kasaliwal, T. Villmow, Establishment, morphology and properties of carbon nanotube networks in polymer melts, Polymer. 53(1) (2012) 4-28. https://doi.org/10.1016/j.polymer.2011.10.063.

[46] M. Liebscher, J. Domurath, B. Krause, M. Saphiannikova, G. Heinrich, P. Pötschke, Electrical and melt rheological characterization of PC and co-continuous PC/SAN blends filled with CNTs: Relationship between melt-mixing parameters, filler dispersion, and filler aspect ratio, J. Polym. Sci. B: Polym. Phys. 56(1) (2018) 79-88. https://dx.doi.org/10.1002/polb.24515.

[47] G. Kasaliwal, T. Villmow, S. Pegel, P. Pötschke, Influence of material and processing parameters on carbon nanotube dispersion in polymer melts, Polymer–Carbon Nanotube Composites, Elsevier, 2011, pp. 92-132. http://dx.doi.org/10.1533/9780857091390.1.92.

[48] S. Wang, R. Liang, B. Wang, C. Zhang, Dispersion and thermal conductivity of carbon nanotube composites, Carbon. 47(1) (2009) 53-57. https://doi.org/10.1016/j.carbon.2008.08.024.

[49] Z. Han, A. Fina, Thermal conductivity of carbon nanotubes and their polymer nanocomposites: A review, Prog. Polym. Sci. 36(7) (2011) 914-944. https://doi.org/10.1016/j.progpolymsci.2010.11.004.

[50] M. Mahmoodi, Y.H. Lee, A. Mohamad, S.S. Park, Effect of flow induced alignment on the thermal conductivity of injection molded carbon nanotube-filled polystyrene nanocomposites, Polym. Eng. Sci. 55(4) (2015) 753-762. http://dx.doi.org/10.1002/pen.23942.

[51] I. Mazov, I. Burmistrov, I. Il'inykh, A. Stepashkin, D. Kuznetsov, J.P. Issi, Anisotropic thermal conductivity of polypropylene composites filled with carbon fibers and multiwall carbon nanotubes, Polym. Compos. 36(11) (2015) 1951-1957. http://dx.doi.org/10.1002/pc.23104.

[52] A.H. Faraji, M. Moradi, M. Goodarzi, P. Colucci, C. Maletta, An investigation on capability of hybrid Nd: YAG laser-TIG welding technology for AA2198 Al-Li alloy, Opt. Lasers Eng. 96 (2017) 1-6. https://doi.org/10.1016/j.optlaseng.2017.04.004.

[53] M. Moradi, A. Hasani, Z. Pourmand, J. Lawrence, Direct laser metal deposition additive manufacturing of Inconel 718 superalloy: Statistical modelling and optimization by design of experiments, Opt. Laser Technol. 144 (2021) 107380. https://doi.org/10.1016/j.optlastec.2021.107380.

[54] M. Moradi, M.K. Moghadam, M. Shamsborhan, Z.M. Beiranvand, A. Rasouli, M. Vahdati, A. Bakhtiari, M. Bodaghi, Simulation, statistical modeling, and optimization of CO_2 laser cutting process of polycarbonate sheets, Optik. 225 (2021) 164932. https://doi.org/10.1016/j.ijleo.2020.164932.

[55] M. Moradi, P.A. MOHAZA, A. KHORAM, An experimental investigation of the effects of fiber laser percussion drilling: Influence of process parameters, Int. J. Advanced Design and Manufacturing Technology. 9 (4) (2016) 7-12. https://admt.isfahan.iau.ir/article_534987.html.

[56] M. Arjmand, T. Apperley, M. Okoniewski, U. Sundararaj, Comparative study of electromagnetic interference shielding properties of injection molded versus compression molded multi-walled carbon nanotube/polystyrene composites, Carbon. 50(14) (2012) 5126-5134. https://doi.org/10.1016/j.carbon.2012.06.053.

[57] M. Mahmoodi, M. Arjmand, U. Sundararaj, S. Park, The electrical conductivity and electromagnetic interference shielding of injection molded multi-walled carbon nanotube/polystyrene composites, Carbon. 50(4) (2012) 1455-1464. https://doi.org/10.1016/j.carbon.2011.11.004.

[58] K. Parmar, M. Mahmoodi, C. Park, S.S. Park, Effect of CNT alignment on the strain sensing capability of carbon nanotube composites, Smart Mater. Struct. 22(7) (2013) 075006. https://doi.org/10.1088/0964-1726/22/7/075006.

[59] F. Gardea, D.C. Lagoudas, Characterization of electrical and thermal properties of carbon nanotube/epoxy composites, Compos. B. Eng. 56 (2014) 611-620. https://doi.org/10.1016/j.compositesb.2013.08.032.

[60] J. Pan, L. Bian, A physics investigation for influence of carbon nanotube agglomeration on thermal properties of composites, Mater. Chem. Phys. 236 (2019) 121777. https://doi.org/10.1016/j.matchemphys.2019.121777.

[61] B. Zhou, W. Luo, J. Yang, X. Duan, Y. Wen, H. Zhou, R. Chen, B. Shan, Thermal conductivity of aligned CNT/polymer composites using mesoscopic simulation, Compos. Part A Appl. Sci. 90 (2016) 410-416. https://doi.org/10.1016/j.compositesa.2016.07.023.

[62] Y. Feng, G. Zhou, G. Wang, M. Qu, Z. Yu, Removal of some impurities from carbon nanotubes, Chem. Phys. Lett. 375(5-6) (2003) 645-648. https://doi.org/10.1016/S0009-2614(03)00947-3.

[63] T. Kolodiazhnyi, M. Pumera, Towards an ultrasensitive method for the determination of metal impurities in carbon nanotubes, Small. 4(9) (2008) 1476-1484. http://dx.doi.org/10.1002/smll.200800125.

[64] H. Liu, Y. Tang, L. Lu, Y. Xie, W. Yuan, G. Chen, J. Li, T. Fu, Investigation on fiber laser cutting of polyacrylonitrile-based carbon fiber tow, J. Mater. Process. Technol. 263 (2019) 151-163. https://doi.org/10.1016/j.jmatprotec.2018.08.015.

[65] A.K. Ghavidel, M. Zadshakoyan, G. Kiani, J. Lawrence, M. Moradi, Innovative approach using ultrasonic-assisted laser beam machining for the fabrication of ultrasensitive carbon nanotubes-based strain gauges, Opt. Lasers Eng. 161 (2023) 107325. https://doi.org/10.1016/j.optlaseng.2022.107325.

[66] M. Hemmati, A. Narimani, H. Shariatpanahi, A. Fereidoon, M.G. Ahangari, Study on morphology, rheology and mechanical properties of thermoplastic elastomer polyolefin (TPO)/carbon nanotube nanocomposites with reference to the effect of polypropylene-grafted-maleic anhydride (PP-g-MA) as a compatibilizer, Int. J. Polym. Mater. 60(6) (2011) 384-397. https://doi.org/10.1080/00914037.2010.531810.

[67] J. Hubbard, J. Tirano, H. Zea, C. Luhrs, Effects of Thermal Activation on CNT Nanocomposite Electrical Conductivity and Rheology, Polymers. 14(5) (2022) 1003. https://doi.org/10.3390/polym14051003.

[68] R. Nadiv, R.M. Fernandes, G. Ochbaum, J. Dai, M. Buzaglo, M. Varenik, R. Biton, I. Furo, O. Regev, Polymer nanocomposites: Insights on rheology, percolation and molecular mobility, Polymer. 153 (2018) 52-60. https://doi.org/10.1016/j.polymer.2018.07.079.

[69] F. Cesano, M.J. Uddin, A. Damin, D. Scarano, Multifunctional conductive paths obtained by laser processing of non-conductive carbon nanotube/polypropylene composites, Nanomaterials. 11(3) (2021) 604. https://doi.org/10.3390/nano11030604.

[70] A.H.A. Hoseini, M. Arjmand, U. Sundararaj, M. Trifkovic, Significance of interfacial interaction and agglomerates on electrical properties of polymer-carbon nanotube nanocomposites, Mater. Des. 125 (2017) 126-134. https://doi.org/10.1016/j.matdes.2017.04.004.

[71] A. Kashyap, N.P. Singh, S. Arora, V. Singh, V. Gupta, Effect of amino-functionalization of MWCNTs on the mechanical and thermal properties of MWCNTs/epoxy composites, Bull. Mater. Sci. 43(1) (2020) 1-9. https://doi.org/10.1007/s12034-019-2012-0.

[72] L.T.M. Hoa, Characterization of multi-walled carbon nanotubes functionalized by a mixture of HNO3/H2SO4, Diam. Relat. Mater. 89 (2018) 43-51. https://doi.org/10.1016/j.diamond.2018.08.008.

[73] M. Kwiatkowska, R. Pełech, A. Jędrzejewska, D. Moszyński, I. Pełech, Different approaches to oxygen functionalization of multi-walled carbon nanotubes and their effect on mechanical and thermal properties of polyamide 12 based composites, Polymers. 12(2) (2020) 308. https://doi.org/10.3390%2Fpolym12020308.